BBA - Bioenergetics 1860 (2019) 601–610

Contents lists available at ScienceDirect

BBA - Bioenergetics

journal homepage: www.elsevier.com/locate/bbabio

Multiple pathways of charge recombination revealed by the temperature dependence of electron transfer kinetics in cyanobacterial photosystem I

Georgy Milanovsky[a,1], Oksana Gopta[a,b,1,2], Anastasia Petrova[a], Mahir Mamedov[a], Michael Gorka[b], Dmitry Cherepanov[c,*], John H. Golbeck[b,d,*], Alexey Semenov[a,c,*]

[a] A.N. Belozersky Institute of Physical-Chemical Biology, Lomonosov Moscow State University, Moscow, Russia
[b] Department of Biochemistry and Molecular Biology, The Pennsylvania State University, State College, PA, USA
[c] N.N. Semenov Institute of Chemical Physics, Russian Academy of Sciences, Moscow, Russia
[d] Department of Chemistry, The Pennsylvania State University, State College, PA, USA

ARTICLE INFO

Keywords:
Electron transfer
Photosystem I
Temperature dependence
Activation energy
Conformational mobility
Glass transition

ABSTRACT

The kinetics of charge recombination in Photosystem I P_{700}-F_A/F_B complexes and P_{700}-F_X cores lacking the terminal iron-sulfur clusters were studied over a temperatures range of 310 K to 4.2 K. Analysis of the charge recombination kinetics in this temperature range allowed the assignment of backward electron transfer from the different electron acceptors to P_{700}^+. The kinetic and thermodynamic parameters of these recombination reactions were determined. The kinetics of all electron transfer reactions were activation-less below 170 K, the glass transition temperature of the water-glycerol solution. Above this temperature, recombination from $[F_A/F_B]^-$ in P_{700}-F_A/F_B complexes was found to proceed along two pathways with different activation energies (E_a). The charge recombination via A_{1A} has an E_a of ~290 meV and is dominant at temperatures above ~280 K, whereas the direct recombination from F_X^- has an E_a of 22 meV and is prevalent in the 200 K to 270 K temperature range. Charge recombination from the F_X cluster becomes highly heterogeneous at temperatures below 200 K. The conformational mobility of Photosystem I was studied by molecular dynamics simulations. The F_X cluster was found to 'swing' by ~30° along the axis between the two sulfur atoms proximal to F_A/F_B. The partial rotation of F_X is accompanied by significant changes of electric potential within the iron-sulfur cluster, which may induce preferential electron localization at different atoms of the F_X cluster. These effects may account for the partial arrest of forward electron transfer and for the heterogeneity of charge recombination observed at the glass transition temperature.

1. Introduction

Photosystem I (PS I) is a key photosynthetic chlorophyll-protein complex that carries out an extremely efficient transformation of light quantum energy into a charge separated state. The PS I reaction center (RC) in cyanobacteria contains six chlorophyll *a* (Chl) molecules, two phylloquinone (PhQ) molecules and three [4Fe-4S] clusters F_X, F_B and F_A (reviewed in [1–3]). The Chls, PhQs and iron-sulfur cluster F_X are bound to the PsaA/PsaB heterodimer and are arranged in two nearly symmetrical branches of redox cofactors, *A* and *B*, that converge at F_X [4–6]. The terminal iron-sulfur clusters F_A and F_B are bound to the extrinsic PsaC subunit [7–9]. The PS I RC also incorporates light-harvesting antenna in the form of 90 Chl *a* and 22 β-carotene molecules that are largely associated with the PsaA/PsaB heterodimer [10].

The excitation of antenna pigments by light quanta leads to ultrafast energy transfer to the RC Chl molecules, where the primary electron donor, a Chl special pair termed P_{700} [11,12], becomes oxidized and the primary Chl acceptor termed A_0 (A_{0A} or A_{0B}) becomes reduced [13–15]. The electron is further transferred to the secondary PhQ molecules (A_{1A} or A_{1B}) [16] and subsequently to the F_X, F_A and F_B iron-sulfur clusters. Both the *A* and *B* branches of redox cofactors are involved in electron transfer (ET) [17], but in cyanobacteria ET is asymmetric in favor of the *A* branch (reviewed in [18]).

In isolated PS I (herein P_{700}-F_A/F_B complexes), the formation of the

Abbreviations: PS I, photosystem I; RC, reaction center; Chl, chlorophyll; ET, electron transfer

* Corresponding authors.
E-mail addresses: cherepanov@genebee.msu.ru (D. Cherepanov), jhg5@psu.edu (J.H. Golbeck), semenov@genebee.msu.ru (A. Semenov).

[1] These authors contributed equally to the article.
[2] On leave from employer.

https://doi.org/10.1016/j.bbabio.2019.06.008
Received 7 March 2019; Received in revised form 22 May 2019; Accepted 15 June 2019
Available online 25 June 2019
0005-2728/ © 2019 Elsevier B.V. All rights reserved.

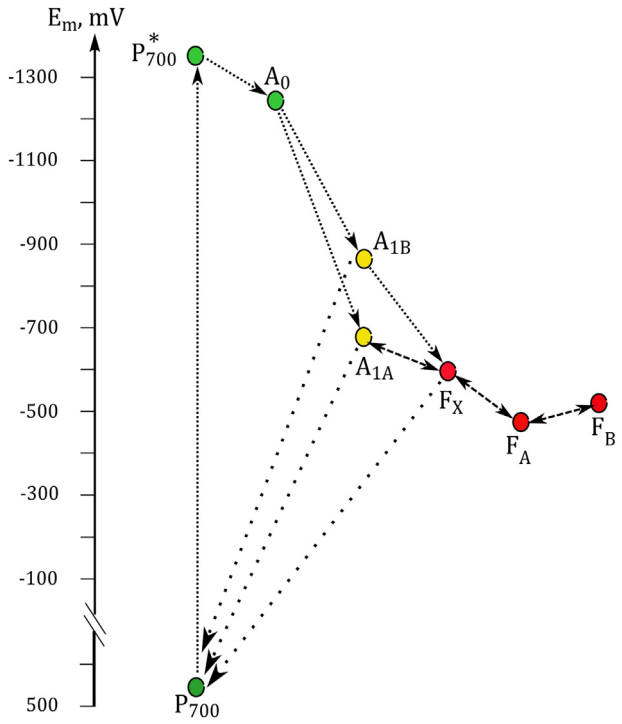

Fig. 1. ET transfer scheme in PS I. The midpoint potentials of the cofactors are shown on the Y-axis. The cofactors of the ET chain are colored according to their identity: chlorophyll (green), phylloquinone (yellow), iron-sulfur cluster (red).

P_{700}^+ $[F_A/F_B]^-$ radical pair occurs in ~200 ns [16]. In the absence of external donors and acceptors, charge recombination between $[F_A/F_B]^-$ and P_{700}^+ occurs with a lifetime of 50 to 100 ms [19,20]. In PS I cores lacking the terminal F_A/F_B clusters (herein P_{700}-F_X core complexes) the lifetime of charge recombination between F_X^- and P_{700}^+ varies in the range of 0.5 to 5 ms [21,22] and in PS I cores lacking all three iron-sulfur clusters (herein P_{700}-A_1 core complexes) the lifetimes of charge recombination between A_1^- and P_{700}^+ were found to be ~10 μs and ~150 μs [23,24]. It was shown that the ~10 μs kinetic component is due to recombination from A_{1B}^- in the *B* branch, while the ~150 μs kinetic component is due to recombination from A_{1A}^- in the *A* branch [24] (Fig. 1).

A number of studies have described the influence of temperature on both the forward and backward ET reactions in PS I. One of the earliest studies showed that at cryogenic temperatures about two-thirds of RCs exhibited irreversible charge separation on successive laser flashes. The remaining one-third of RCs showed several broadly distributed recombination lifetimes ranging from 120 μs to 500 ms [25]. It was later observed that recombination between A_0^- and P_{700}^+ has a slight temperature dependence in enriched spinach PS I that lacked a quinone in the A_1 site [26]. Specifically, the half-life of the recombination reaction slowed from ~47 ns at room temperature to ~82 ns at 10 K.

The temperature dependence of the reoxidation from the quinone acceptor, A_1, has been the most thoroughly investigated of any cofactor. PhQ reoxidation studies clearly show a temperature dependence of the $A_1^- \rightarrow F_X$ electron transfer process [27,28]. Interestingly, it appears that only the $A_{1A}^- \rightarrow F_X$ reaction is thermally activated (E_a = 110 meV), while the $A_{1B}^- \rightarrow F_X$ reaction remains nearly temperature independent, with an E_a of 15 meV [28]. A further lowering of the temperature led to inefficiencies in forward ET, resulting in 45% of the electrons blocked at A_1, and 20% at F_X at temperatures below 150 K [2,27]. An early study on recombination rates between A_1^- and P_{700}^+ showed only a moderate ~1.5-fold slowing of the rate upon lowering the temperature, though this study was unable to distinguish between the two branches [27]. A more recent study on genetically produced P_{700}-A_1 cores showed that recombination is not only moderately slowed in each branch, but the relative amplitude of each branch also changes as temperature is decreased [24]. A separate study revealed the inverse effect of increasing the recombination rate between A_1^- and P_{700}^+ as the temperature was lowered, however the PS I being analyzed contained non-native high-potential quinones in the A_1 site [29].

In contrast to these simplified systems containing only A_0 and A_1, less is known about temperature dependences or recombination pathways involving the F_X, F_A, and F_B iron-sulfur clusters. Recombination between F_X^- and P_{700}^+ is thermally activated, suggesting that it occurs via the intermediate state of P_{700}^+ and A_1^- [2,30,31]. Analyzing the recombination reaction between $[F_A/F_B]^-$ and P_{700}^+ at temperatures from 275 K to 306 K showed that this process is also thermally activated, having an activation energy of 220 meV [32]. Clearly, the addition of three unique iron-sulfur clusters in an extended ET chain significantly complicates the analysis of the temperature dependence.

The present work aims to elucidate the kinetic and thermodynamic effects of temperature, from 310 K to 4 K, for P_{700}-F_A/F_B complexes and P_{700}-F_X cores in a water-glycerol glassy matrix. By taking measurements at 10 K increments from ~310 K to 4 K, the change in kinetics can be plotted as a function of temperature, which allows for several unique observations. At temperatures below 200 K, P_{700}-F_X cores exhibit broadly distributed recombination reactions over several orders of magnitude. We suggest that this is caused by different orientations of F_X, which gives rise to differential electron localization on the atoms of the iron-sulfur cluster. Further, charge recombination from F_A/F_B is demonstrated to occur via two unique pathways, each with a different activation energy. At high temperatures (> 280 K), recombination occurs via ET to the A_{1A} PhQ, with an activation energy of ~290 meV. At temperatures from 200 to 270 K, direct recombination from F_X^- is proposed to occur with an activation energy of ~22 meV.

2. Materials and methods

2.1. Cell growth and isolation of thylakoids and PS I trimers

Cells of *Synechocystis* sp. PCC 6803 were grown at 30 °C in BG-11 medium under light. The culture in late exponential phase was pelleted by centrifugation, washed twice with BG-11 medium, and suspended in 50 mM HEPES-NaOH buffer (pH 7.5). P_{700}-F_A/F_B trimers were isolated using n-dodecyl-β-d-maltoside (β-DDM) and sucrose density gradients as described previously [33], resuspended in 50 mM Tris, pH 8.0, containing 0.03% (w/v) β-DDM and 15% (v/v) glycerol at a Chl concentration of 1.5 to 2 mg ml^{-1}, and stored at −80 °C. Preparation of P_{700}-F_X core complexes was performed by incubation of PS I complexes in 50 mM Tris, pH 8.0 buffer containing 6 M urea [22,34].

2.2. Flash-induced transient absorption spectroscopy in the near-IR

Most measurements were made at 820 nm with a laboratory-built spectrometer at Penn State University [20]. The transient absorption kinetics of P_{700}-F_A/F_B complexes and P_{700}-F_X cores were measured in the temperature range from 5 K to 300 K. The PS I preparations were suspended in water-glycerol mixture to ensure the formation of a transparent glass at low temperatures. The glass transition properties of the water-glycerol mixture used in our experiments have been previously characterized [35]. For measurements of the transient absorption kinetics, P_{700}-F_A/F_B complexes and P_{700}-F_X cores were diluted in a buffer containing 50 mM Tris-HCl, pH 8.0, 0.04% β-DDM and ca. 75% (v/v) glycerol, and supplemented with the redox mediators DCPIP (30 μM), and sodium ascorbate (0.5 mM). The samples were placed in a 1 cm by 1 cm polycarbonate cuvette that was modified and sealed to fit the sample cryostat (Janis, MN). Liquid helium was used to cool the samples and the temperature was varied using a Lakeshore auto-sensor temperature controller in 10 K increments, from 10 K to 320 K. A diode

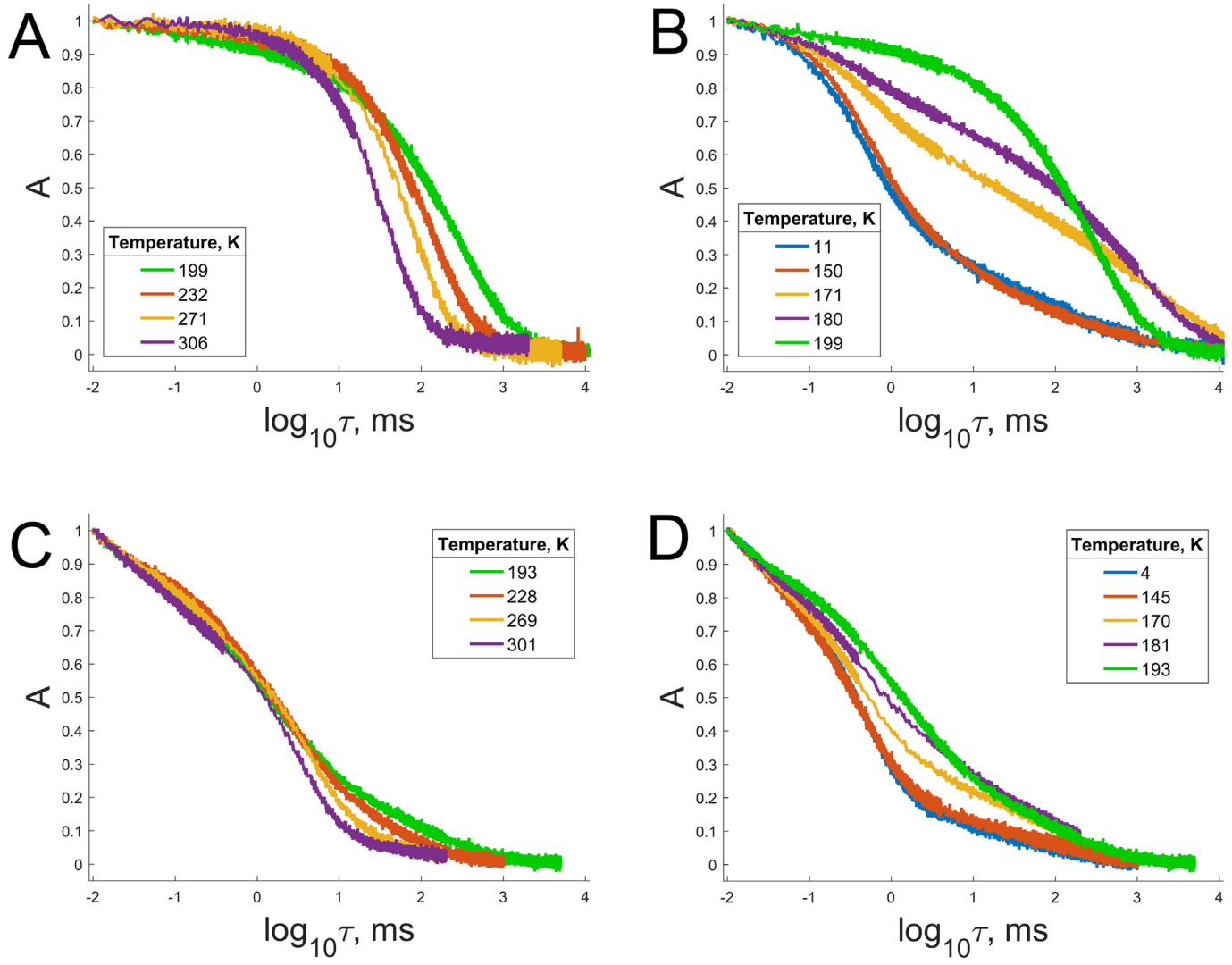

Fig. 2. P_{700}^{+} recombination kinetics in P_{700}-F_A/F_B complexes (A, B) and in P_{700}-F_X cores (C, D) at different temperatures.

laser at 820 nm (Spindler-Hoyer) was used as the measuring beam (5 mW output power) and the samples were excited by a 1 mJ/cm^2 energy pulse from a Nd-YAG laser (Spectra physics, CA) operating at 532 nm with a 7 ns pulse duration. Additional measurements in the temperature range of 260 to 320 K were made at Moscow State University with smaller temperature steps of 3 K using a VWR 1160S thermostat. The light-induced absorption changes were monitored with a single-beam differential spectrophotometer. For this high-temperature region, an LED (830 nm) was employed as a source of the measuring beam. Saturating flashes (532 nm, 15 ns pulse half-width, 40 mJ flash energy) were obtained from a frequency-doubled Nd:YAG laser (Quantel Laser, Les Ulis, France).

2.3. CONTIN analysis of PS I charge recombination kinetics

The kinetics of P_{700}^{+} recombination at low temperature were found to be significantly heterogeneous and could not be properly approximated as a simple sum of exponential components. Thus, the recombination kinetics were analyzed using the CONTIN algorithm [36]. The method implements the inverse Laplace transform to deconvolute monotonous decay kinetics into a spectrum of exponential components without a priori knowledge of the number of distinct peaks. This method is described in detail in our previous work on charge recombination in PS I complexes from the *rubA* mutant of cyanobacteria [24]. The CONTIN kinetic spectrum was separated into individual components in accordance with the original algorithm. See Supplementary Materials for a comparison between the CONTIN deconvolution and a multiexponential approximation of the low-temperature kinetics.

2.4. Molecular dynamics simulation

Molecular dynamics simulations were carried out with a model based on the structure of PS I [10] from the cyanobacterium *Thermosynechococcus elongatus* (PDB ID: 1JB0). The structure included eight main protein subunits (from A to J), 90 Chls, 2 PhQs, 3 iron-sulfur clusters and 19 β-carotenes. The PS I complex together with crystallographic water was embedded in a hydrated lipid bilayer, which was constructed from a typical bacterial phospholipid, 1-palmitoyl-2-oleoyl-sn-glycero-3-phosphocholine. In total, the system included 213 molecules of phospholipid, ~27,000 water molecules and 77 monovalent ions, making ~153,600 atoms. The equilibration of the system was carried out in three stages: first, the lipid was relaxed at the fixed conformation of protein and constrained water positions; next the water was relaxed but the general conformation of PS I was conserved by applying restrictions to C_α atoms of backbone; and finally, a free simulation of the system at 298 K was performed for 10 ns. The subsequent 16 ns trajectory of free dynamics was used for the analysis, and

no drift of potential energy or systematic changes of the system volume (ca. 13.6 × 10.9 × 10.0 nm) were observed. The integration step was 2 fs. Parameterization of atomic interactions for the protein in PS I was based on AMBER molecular potentials [37]. The molecular potentials of chlorophylls and β-carotenes were taken from potentials computed for similar cofactors in PS II [38]. Molecular dynamics simulations were conducted using the Gromacs 5.1 program [39] on the "Lomonosov" supercomputer in the Moscow State University Computing Center. The molecular dynamics simulation step was 2 fs. A constant pressure of 1 atm was maintained at all stages of the simulation; the temperature was kept at 298 K; and the volume of the system was changed independently and without restriction in all dimensions by the Nose–-Hoover Langevin piston method. The results of the molecular dynamics simulations were studied using the VMD program [40]. The primary analysis of trajectory files was performed in MATLAB using laboratory-developed scripts.

3. Results

The kinetics of P_{700}^+ reduction in PS I complexes from the cyanobacterium *Synechocystis* sp. PCC 6803 with varying number of electron acceptors (P_{700}-F_A/F_B complexes and P_{700}-F_X cores lacking the terminal F_A/F_B clusters) were measured by monitoring flash-induced absorption changes at 820 nm over a temperature range of 4 K to ~310 K.

3.1. Charge recombination kinetics in P_{700}-F_A/F_B complexes

The charge recombination kinetics in P_{700}-F_A/F_B complexes are shown in Fig. 2. At temperatures between 310 K and 200 K, a classic temperature-dependent slowing of the kinetics is observed (Fig. 2A). At temperatures between 200 K and 150 K, an abrupt increase in the rate of charge recombination from seconds to milliseconds occurs, whereas below 150 K, the kinetics are almost temperature-independent (Fig. 2B).

The kinetics cannot be adequately described by a simple sum of exponential components and their analysis requires a continual Laplace-type deconvolution. However, the deconvolution of these complex decay kinetics into underlying concurrent processes using the inverse Laplace transform is a non-trivial problem. We employed CONTIN [36], a regularization algorithm that yields quasi-continuous lifetime distributions. Fig. 3 shows a heatmap of P_{700}^+ recombination

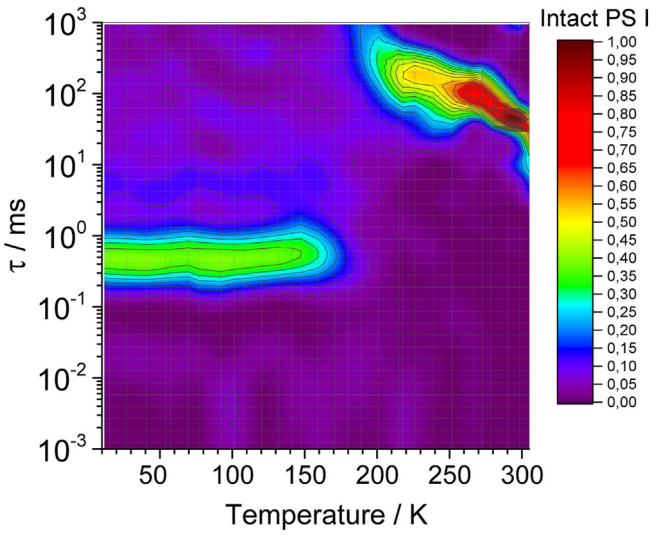

Fig. 3. Heatmap of P_{700}^+ reduction kinetics in P_{700}-F_A/F_B complexes at different temperatures obtained by CONTIN Laplace deconvolution. The violet background denotes zero level. Increasing amplitudes are shown in blue/green/yellow/red, with total amplitude normalized at any given temperature.

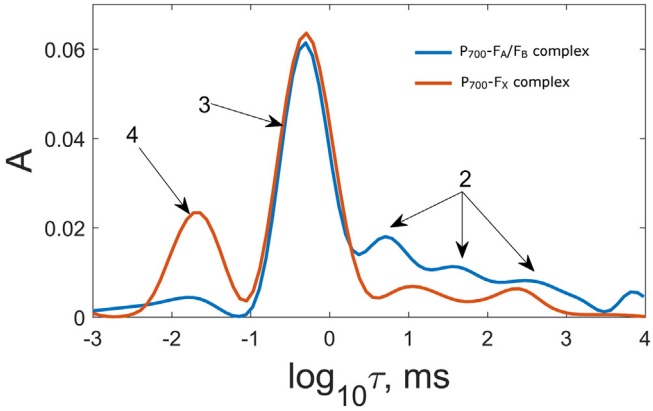

Fig. 4. Distribution of the recombination kinetic components in P_{700}-F_A/F_B complexes (blue) and P_{700}-F_X cores (red) below the glass transition temperature ($T < 170$ K). The peaks ascribed to components *2*, *3* and *4* are labeled.

lifetimes in P_{700}-F_A/F_B complexes in a broad temperature range obtained by CONTIN. The abrupt transition from a temperature-dependent to a temperature-independent process can be readily seen in this depiction. At temperatures below 150 K, ET processes obey heterogeneous distributions that likely reflect the freezing of the protein complex in various conformations. The blue trace in Fig. 4 shows typical CONTIN profile at temperatures lower than 150 K, demonstrating the highly distributed recombination reactions in the time range slower than ~3 ms.

Fig. 5A and B shows the temperature dependence of the mean lifetimes (A) and relative amplitudes (B) of the individual kinetic constituents, selected as peaks from the CONTIN kinetic spectra in accordance with the original algorithm. At temperatures between 310 K and 200 K, the recombination kinetics were well approximated by single exponential components (relative amplitude > 90%) with lifetimes increasing from 25 to 100 ms (component *1*, blue, Fig. 5A, B). The slope of this dependence varies: in the temperature range of 310 K to 280 K, the recombination kinetics were characterized by a high activation energy of ~290 meV, while in the temperature range of 270 K to 200 K, the activation energy was much lower, at 22 meV (see Fig. S1 in Supplementary Materials). Below 200 K, several new kinetic components appeared at the expense of component *1*, which sharply decreased and simultaneously slowed down to several seconds. The two main components are characterized by lifetimes in the range of 15 to 50 ms (a widely distributed component *2*, green) and 300 to 400 μs (component 3, red), with relative amplitudes of 30% and 60%, respectively. A fast component with a lifetime of ~2 to 30 μs was transiently observed below 200 K with a small but discernible amplitude (~5%, component 4, ochre). All of the kinetic components were nearly temperature-independent below 150 K.

3.2. Charge recombination kinetics in P_{700}-F_X cores

The temperature dependence of charge recombination in P_{700}-F_X cores demonstrates common trends with those of P_{700}-F_A/F_B complexes. At temperatures between 300 K and 200 K, a temperature-dependent slowing of the kinetics was observed (Fig. 2C). At temperature between 200 K and 150 K, a slowing in the rate of charge recombination from milliseconds to seconds occurs, whereas below 150 K, the kinetics remain almost temperature-independent (Fig. 2D). Fig. 6 shows the heatmap of P_{700}^+ recombination lifetimes obtained by CONTIN for P_{700}-F_X cores. The abrupt transition from a mildly temperature-dependent to a temperature-independent process can readily be seen in this depiction.

Fig. 5C and D shows the corresponding mean lifetimes (C) and relative amplitudes (D) of the individual kinetic components. Compared

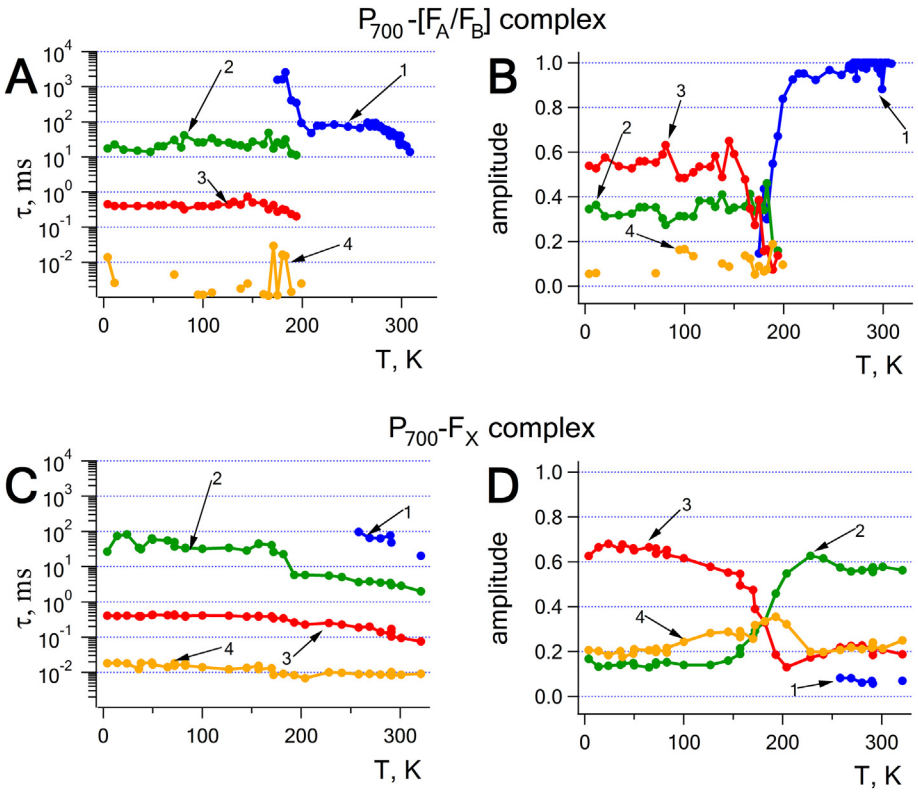

Fig. 5. P_{700}^{+} reduction kinetics (A/C) and component amplitudes (B/D) in P_{700}-F_A/F_B complexes and P_{700}-F_X cores at different temperatures for F_A/F_B (*1*, blue) F_X (*2*, green), A_{1A} (*3*, red) and A_{1B} (*4*, ochre).

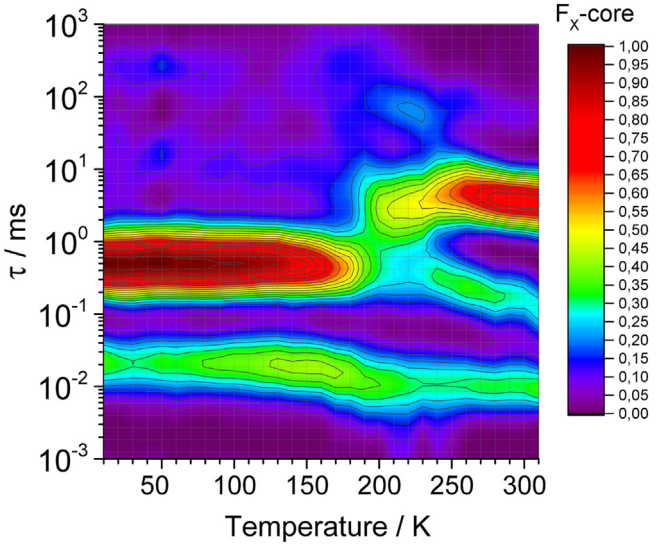

Fig. 6. Heatmap of P_{700}^{+} reduction kinetics in P_{700}-F_X cores at different temperatures obtained by CONTIN Laplace deconvolution. The blue background denotes zero level. The increasing amplitudes are shown in green/yellow/red, with total amplitude normalized at any given temperature. Lines are only drawn between the yellow points in those intervals where the fast kinetic phase could be resolved.

to P_{700}-F_A/F_B complexes, the temperature dependence of charge recombination in P_{700}-F_X cores is more diversified. All visible components are nearly temperature-independent below 150 K. The main kinetic component undergoes apparent bifurcation in the temperature range from 200 K to 150 K (see Fig. 6), a finding that requires a detailed assignment of all observable components. Three components with lifetimes in the time windows of 3 to 100 ms (roughly corresponding to component *2* in P_{700}-F_A/F_B complexes), 100 to 400 µs (equivalent to component *3* in P_{700}-F_A/F_B complexes) and 10 to 20 µs (equivalent to the fast component *4* in P_{700}-F_A/F_B complexes) were observed throughout the entire temperature range. The slowest component *1*, observed in the recombination kinetics in P_{700}-F_A/F_B complexes above 200 K, was only observed at temperatures above 250 K, and corresponds to < 10% of the total amplitude. The second slowest component *2* becomes notably heterogeneous at low temperatures and cannot be unequivocally described as a sum of exponential kinetics (Fig. 4, red trace). The green line 2 at Fig. 5C denotes the mean weighted average lifetime of this component.

At temperatures higher than 200 K, component *2* has a relative amplitude of 55–60% and a characteristic lifetime that increases from ~3 ms at room temperature to 10 ms at 200 K corresponding to an activation energy of ~100 meV (see Table 1). On lowering the temperature below ~200 K, the contribution of component *2* decreased to ~20% of the total amplitude, whereas the contribution of the faster component *3* increased from ~25% to 65% of the total amplitude. The amplitudes of components *2* and *3* remained nearly unchanged on lowering the temperature below 150 K. The fastest component *4* (lifetime 10 to 20 µs) retained the same relative amplitude of ~20% throughout the entire temperature range. The kinetics of components *3* and *4* were almost temperature-independent, slowing by about a factor of three over the temperature range of 300 K to 200 K with activation energy of 30 meV.

Table 1
Activation energy of P_{700}^{+} recombination reactions in P_{700}-F_A/F_B complexes and P_{700}-F_X cores (at $T > 200$ K).

Sample	Reaction	E_a, mV
P_{700}-F_A/F_B complexes	$P^{+}[F_A/F_B]^{-} \rightarrow P\,[F_A/F_B]$, $T > 280$ K	290
	$P^{+}[F_A/F_B]^{-} \rightarrow P\,[F_A/F_B]$, $T < 270$ K	22
P_{700}-F_X cores	$P^{+}F_X^{-} \rightarrow P\,F_X$	100

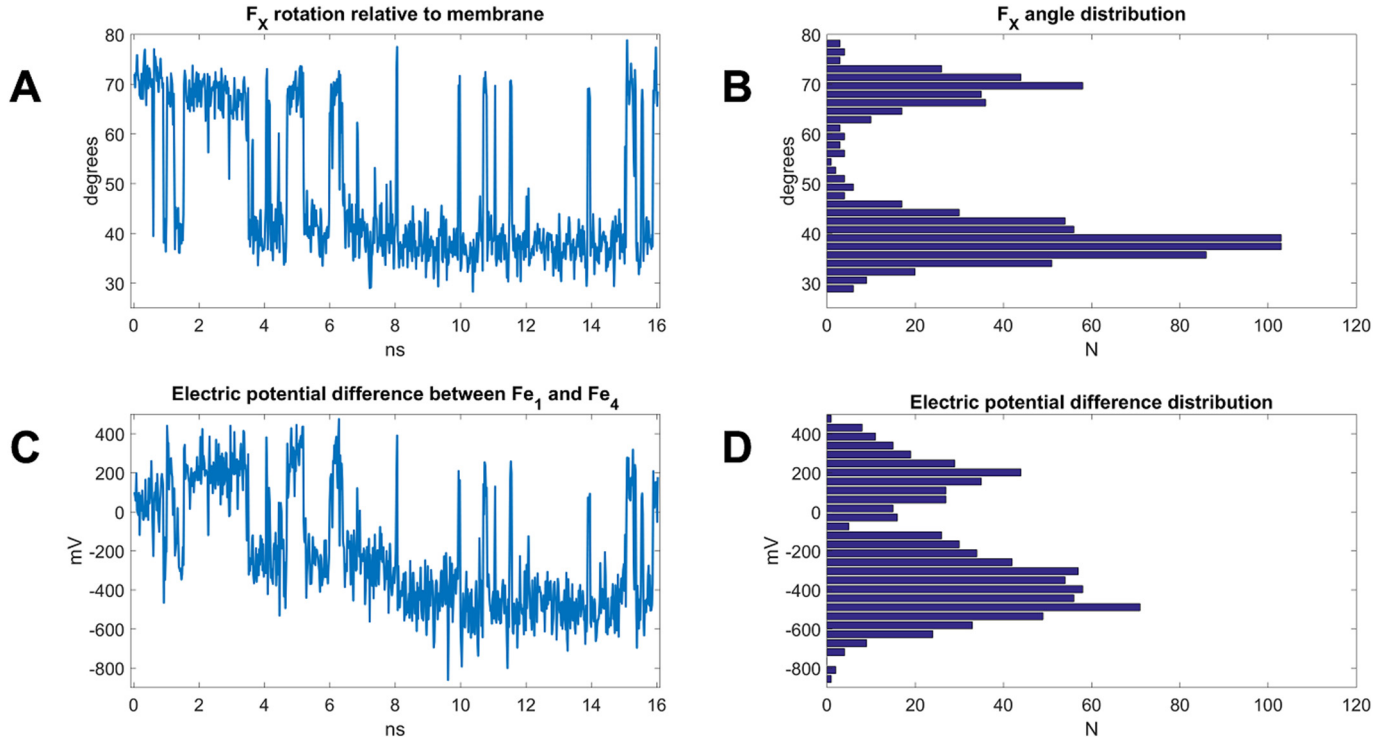

Fig. 7. Conformational mobility of the F_X cluster. Dynamics (A) and distribution (B) of the angle between the membrane plane and the S_1-S_2-S_3 plane of the cluster are shown. Dynamics (C) and distribution (D) of electric potential difference between the Fe_1 and Fe_4 atoms of the F_X cluster demonstrate the resulting change of electric field intensity.

3.2.1. *Molecular dynamics modelling of PS I*

To uncover a basis for the experimentally observed multiple recombination modes that result in heterogeneous ET reactions at low temperature, we conducted molecular dynamics (MD) modelling of the PS I complex, employing an expanded model from a previously published simulation of the same complex [41]. The F_X cluster was found to undergo significant conformational changes during the free 16 ns duration molecular dynamics trajectory at room temperature. The internal geometry of the cluster itself was stable, but the relative orientation of the tetrahedral cluster, in relation to the surrounding protein matrix and normal to the membrane plane, fluctuated between two distinct conformations. Fig. 7A depicts the changes of the angle measured between the normal to the membrane plane and the plane containing the S_1, S_2 and S_3 sulfur atoms of the F_X cluster over a 16 ns long MD trajectory, while Fig. 7B shows a histogram of the same data. Calculating the correlation between this angle and the coordinates of the protein backbone C_α atoms revealed that the rotation is coupled with local lateral movements of the protein loop containing residues 560–567 of protein subunit B (see Fig. S2 in Supplementary Materials). Cysteine residue Cys565B acts as a bearing point for these movements.

Although the observed F_X conformational changes had an amplitude of < 1.5 Å, they are coupled with significant changes of electric potential of the F_X cluster atoms. The electric potential from the whole protein complex (with the exception of the F_X cluster itself) was calculated at the various atoms of F_X. Correlation coefficients between the rotation of the cluster and the dynamics of the electric potentials at different cluster atoms varied from zero to 0.9 (see Table S1 in supplementary materials). The two atoms with the highest correlation between electric potential fluctuations and the conformational state of the F_X cluster were found to be the Fe_1 and Fe_4 iron atoms (Fig. 8); the electric potential changes at these atoms are opposite to each other, indicating the existence of an electric field at these atoms (Table S1). The difference in the changes of electric potentials at these atoms is plotted in Fig. 7C and a histogram of this data is shown in Fig. 7D.

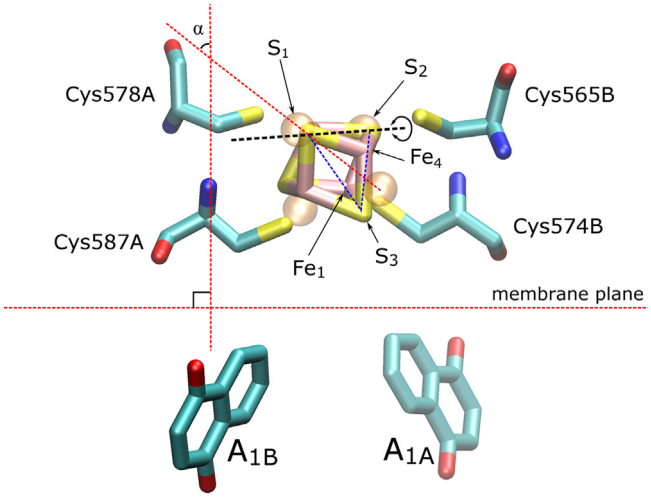

Fig. 8. Structural model of the F_X cluster. Individual atoms, mentioned in the text, are marked with arrows. The secondary electron acceptors, A_{1A}/A_{1B}, and the cysteine residues that coordinate the F_X cluster, are shown as licorice models. Alternate positions of the sulfur atoms of the F_X cluster are shown as semi-transparent spheres with the rotational axis marked in black dashed line. The angle between the S_1-S_2-S_3 plane of the F_X cluster and the membrane plane normal (see Fig. 7A) is shown as α.

4. Discussion

4.1. *Assignment of the kinetic components*

The results presented above clearly demonstrate the existence of several distinct charge recombination reactions in PS I. Their origin can be derived from the scheme of ET presented in Fig. 1. Based on energetics, direct recombination to P_{700}^+ is possible from two cofactors, A_{1A} and F_X, whereas recombination from the F_A/F_B cluster is only

possible through the intermediate state of $P_{700}^{+}F_X^{-}$ (and via $P_{700}^{+}A_{1A}^{-}$) due to the large distance between the terminal iron-sulfur clusters and P_{700}. Charge recombination through formation of the intermediate state $P_{700}^{+}A_{1B}^{-}$ is energetically unlikely, as the A_{1B} PhQ has a lower redox potential than both A_{1A} and F_X [42–44].

4.1.1. P_{700}-F_X cores

The faster components of P_{700}^{+} recombination kinetics in P_{700}-F_X cores are similar to those in P_{700}-A_1 cores from the *rubA* deletion mutant, as previously reported [24]; however, recombination kinetics of P_{700}-F_X include an additional component *2*, which can be assigned to the recombination between P_{700}^{+} and F_X^{-} (Fig. 5C, D). While the kinetics of components *3* and *4* (recombination reactions from A_{1A}^{-} and A_{1B}^{-} with lifetimes of ~100 to 300 µs and ~10 to 20 µs, respectively [45]) can be considered as mono-exponential, component *2* cannot be described as a simple exponential process. It instead represents a heterogeneous reaction with broadly distributed kinetics (see Fig. 4 and the dark blue areas at the top side of Fig. 6) with a weighted average lifetime that varies from 4 ms at 310 K to ~100 ms at temperatures below 150 K. The heterogeneity of this reaction increases below 250 K, which likely reflects the immobilization of the protein in conformational states with distinct reaction rates.

Considering that almost no recombination is observed from A_{1B}^{-} in P_{700}-F_A/F_B complexes at temperatures below 150 K (see Fig. 3), the observed 20% amplitude of A_{1B}^{-} recombination in P_{700}-F_X cores (see Fig. 5D) requires an explanation. It is known that the F_X iron-sulfur cluster is destroyed in a fraction of PS I during the removal of the PsaC protein, and in these RCs forward ET is blocked beyond A_1. In a previously published study, destruction of ~25% of the F_X clusters was reported during preparation of F_X-cores [20]. The recombination from reduced PhQ in either the *A* or *B* branch at temperatures higher than 150 K (components *3* and *4*) accounts in this case for ~40% of the total absorption change, reflecting the amount of damaged P_{700}-F_X cores in this preparation. Assuming that all recombination from A_{1B}^{-} occurs in PS I complexes lacking F_X, the data suggest that almost all of the electrons in undamaged P_{700}-F_X cores recombine from the F_X cluster at temperatures above 200 K, while below 150 K they recombine from A_{1A} and F_X in a ratio of 2:1, similar to P_{700}-F_A/F_B complexes (see Fig. 5B, D). Based on its lifetime [2,20] and amplitude, component *1* is due to recombination from $[F_A/F_B]^{-}$ in those RCs in which a small amount of PsaC was retained.

4.1.2. P_{700}-F_A/F_B complexes

The kinetics of P_{700}^{+} recombination in P_{700}-F_A/F_B complexes at low temperatures show common characteristics to those in P_{700}-F_X cores (Fig. 4). However, the predominant recombination kinetic component (component *1*), observed at temperatures above 200 K (Fig. 5A), is approximately an order of magnitude slower than the main recombination component observed in P_{700}-F_X cores (component *2*, Fig. 5C). Component *1* can be assigned to the back reaction from the terminal iron-sulfur clusters $[F_A/F_B]^{-}$ to P_{700}^{+} on account of its characteristic lifetime [2,20]. Based on its temperature dependence, it has an activation energy $E_a \approx 290$ mV at $T > 280$ K and $E_a \approx 22$ mV at $200\ K < T < 270$ K (see Table 1 and Fig. S1 in Supplementary Materials). The former value is roughly comparable to the $E_a \approx 220$ mV of the recombination between the F_A/F_B clusters and P_{700} reported by [32]. The bend in the temperature dependence of the $[F_A/F_B]^{-} \rightarrow P_{700}^{+}$ recombination kinetics around 280 K probably reflects a change in the charge recombination mechanism: at T > 280 K the reaction occurs via intermediate reduction of A_{1A}, whereas below 270 K the direct recombination from F_X^{-} to P_{700}^{+} rationalizes the small activation energy of recombination.

Component *3*, which is assigned to recombination from A_{1A}^{-}, becomes predominant at temperatures < 150 K, with almost 60% of electrons trapped at the A_1 level. They are not passed forward to the iron-sulfur clusters, a finding consistent with previous reports [46–50]. The minor component *4* is attributed to charge recombination between A_{1B}^{-} and P_{700}^{+} based on its similarity to a corresponding recombination component in P_{700}-F_X cores [45] and P_{700}-A_1 cores [24]. The assignment of the slower kinetic phase to the recombination between A_{1A}^{-} and P_{700}^{+} and the faster kinetic phase to the recombination between A_{1B}^{-} and P_{700}^{+} agrees with studies of the decay of the electron spin echo signal derived from the $P_{700}^{+}A_1^{-}$ radical pair in wild-type and PS I at 100 K, which indicated that the loss of spin coherence decays an order of magnitude faster from the $P_{700}^{+}A_{1B}^{-}$ state than from the $P_{700}^{+}A_{1A}^{-}$ state [51,52].

Component *2* is ascribed to charge recombination between the iron-sulfur cluster F_X^{-} and P_{700}^{+}, and as indicated above, component *3* to charge recombination between quinone A_{1A}^{-} and P_{700}^{+} [2,20,49,53]. The kinetics of the $P_{700}^{+}F_X^{-}$ recombination reaction has a broad distribution at low temperatures (especially visible in P_{700}-F_X cores), which likely reflects the freezing-in of various PS I conformational substates. A similar non-exponential behavior of charge recombination kinetics was observed in the purple bacterial RC at low temperature [54] and explained by a two-fold distribution of the quinone position in the protein. However, in contrast to the quinone in the bacterial RC, both the iron-sulfur clusters and the PhQs in PS I are anchored in the protein matrix [41] and, within the error of the measurement, no discernable changes in the distance between the redox cofactors have been detected by high-field EPR measurements at low temperature [21,55,56].

Parameters of the discovered kinetic components of P_{700}^{+} recombination in PS I complexes with different number of iron-sulfur clusters can be found in Table 2.

4.2. Molecular dynamics simulation of the conformational mobility of PS I

We applied a MD model of PS I to study the conformational mobility of the protein complex in the neighborhood of the [4Fe-4S] clusters in an attempt to elucidate the heterogeneity of charge recombination from the F_X cluster at low temperatures. This effect was observed both in P_{700}-F_A/F_B complexes and P_{700}-F_X cores (Fig. 4). The F_X cluster

Table 2
Kinetic characteristics of P_{700}^{+} recombination reaction components in P_{700}-F_A/F_B complexes (this work), P_{700}-F_X cores (this work), and P_{700}-A_1 cores (see ref. [24]) in different temperature ranges.

Sample	T, K	P_{700} recombination components									
		F_A/F_B		F_X distal		F_X proximal		A_{1A}		A_{1B}	
		A, %	τ, ms	A, %	τ, ms	A, %	τ, ms	A, %	τ, ms	A, %	τ, ms
P_{700}-F_A/F_B	4–150	n/a		9	> 2500	29	45	59	0.44	3	0.024
	200–320	97	57	n/a		n/a		n/a		n/a	
P_{700}-F_X	4–150	n/a				15	104	65	0.41	20	0.019
	250–320					55	5.58	26	0.21	19	0.01
P_{700}-A_1	4–100	n/a						73	0.263	27	0.018
	150–290							57	0.189	43	0.013

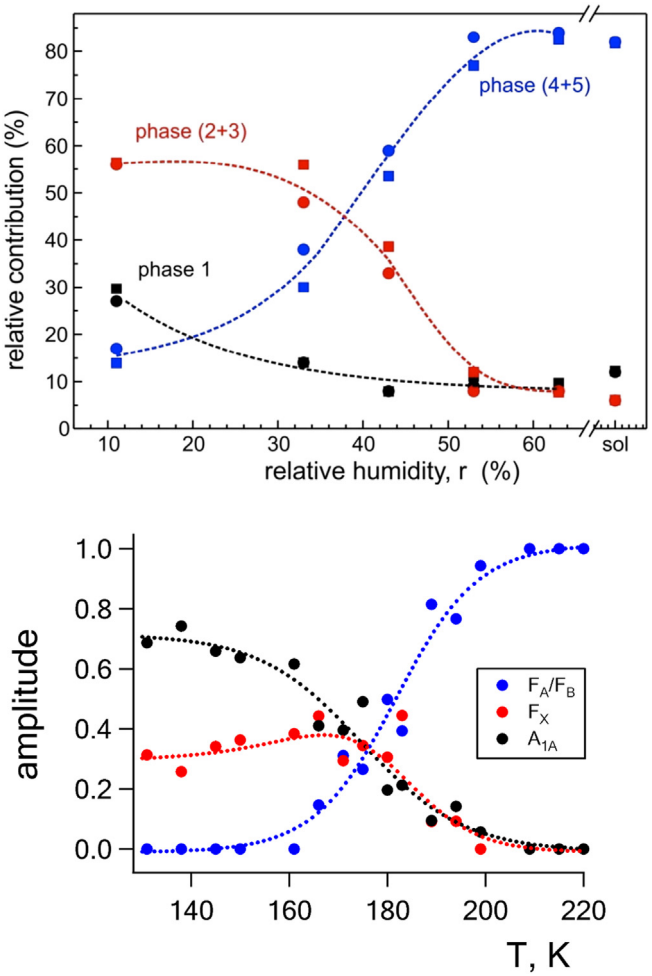

Fig. 9. Recombination components of PS I in a glassy matrix. Top Panel: temperature dependence of the relative amplitudes of distinct kinetic components in water-glycerol solution (data identical to Fig. 4B, components of recombination from A_{1A}, F_X and F_A/F_B are shown); Bottom Panel: dependence of relative amplitudes of kinetic components on the humidity of the protein-trehalose glassy matrix at room temperature (reproduced from ref. [21]. Phases 4 + 5 are attributed to recombination from F_A/F_B, phases 2 + 3 to F_X and phase 1 to A_{1A}).

switched its conformation between two distinct positions multiple times during 16 ns MD trajectory (Fig. 7A). This mobility results from the rotation of the F_X cluster around the axis between the S_1 and S_2 sulfur atoms (Fig. 8) and is accompanied by lateral mobility of a nearby protein loop (Fig. S1). The swinging motion correlated with changes of electrostatic potential differences between the two iron atoms Fe_1 and Fe_4 of the F_X cluster (Fig. 7C).

Such notable changes of electrostatic potential can result in a significant redistribution of spin and electron density within the iron-sulfur cluster. Bominaar and coauthors [57] performed DFT calculations of the electron density distribution within [4Fe-4S] clusters and found that intramolecular spin-dependent electron delocalization has an impact on the rate constant for intermolecular ET. The dependence of charge distribution within [4Fe-4S] clusters on electrostatic fields and dielectric properties of the environment suggests that an exchange-coupled F_X cluster can act as a molecular switch in exchange-controlled electron gating. This switch can alter both the reorganization energy and the electronic coupling between redox cofactors [57].

At high temperature, switching between different conformations of the F_X cluster occur on a nanosecond time scale (Fig. 7A), which is much faster than ET from $[A_{1A}/A_{1B}]^-$ to F_X and from F_X^- to F_A/F_B (even more so for slower recombination reactions from F_X^- to P_{700}^+). This mobility becomes severely limited when the temperature is lowered below the glass transition point of the water-glycerol solution used in this study. This is accompanied with an experimentally-observed partial arresting of both forward ET from $[A_{1A}/A_{1B}]^-$ to F_X (Fig. 5B, D, red traces) and from F_X^- to F_A/F_B (Fig. 5B, blue trace). We propose that these processes are connected. The individual protein complexes become immobilized in one of two states, (i) with ET allowed from A_1^- to F_X or (ii) from F_X^- to F_A/F_B. At high temperatures, ET from A_1^- to F_A/F_B is not limited by F_X conformations, but below the glass transition temperature, the F_X cluster becomes a molecular switch, locking the PS I complex in a state either incapable of F_X reduction altogether or preventing forward ET from reduced F_X to F_A/F_B. In the latter case, rate of recombination reaction $F_X^- \rightarrow P_{700}^+$ becomes heterogeneous due to a multifold of conformational states. This conformational mobility can be associated with large entropy changes observed for ET reactions related to the iron-sulfur clusters of PS I [58]. Nevertheless, the F_X cluster may not be the only protein domain that becomes immobilized in a variety of substates upon freezing, and other sources could lead to kinetic heterogeneity in the ET processes. However, no other dramatic conformational changes were detected in the MD model employed in the study.

Concerning the conformational mobility of the F_X cluster, it should be noted that its EPR spectrum shows considerably broader *g*-anisotropy in P_{700}-F_X cores than in intact P_{700}-$[F_A/F_B]$ cores. This has been historically attributed to the freezing-in of a greater number of conformational states of F_X cluster when the stabilizing effect of the PsaC, PsaD, and PsaE proteins are absent [22,59]. Here, we provide a mechanistic basis for the presence of two different conformational states of the F_X cluster. Accordingly, the broader spectrum of the F_X cluster would represent the admixture of these two major conformational states plus additional minor conformational states that might not be resolved by the molecular mechanics calculations. Moreover, the EPR spectrum of the F_A/F_B clusters, recently obtained on PS I complexes immobilized in a trehalose glass, were different from the EPR spectra obtained at low temperatures in frozen solution [45]. It is therefore possible that the EPR spectrum of the F_A/F_B clusters also represent an admixture of the spectra of different possible conformations.

4.3. Comparison with room temperature trehalose glasses

Much like the water-glycerol system, solutions of various saccharides, such as trehalose (α-D-glucopyranosyl-(1 → 1)-α-D-glucopyranoside), are used to preserve the structure and functionality of proteins under stress conditions, e.g. low and high temperature and humidity [60,61]. It is therefore interesting to compare the effects of a low temperature water-glycerol mixture with other methods that restrict protein conformational mobility. A number of similarities are immediately apparent in the charge recombination kinetics of PS I immobilized in glycerol glass at 170 K (this work) and trehalose glass at 298 K [45,62]. The first is that in each PS I preparation (P_{700}-F_A/F_B complexes, P_{700}-F_X cores, and P_{700}-A_1 cores), ET is blocked to different amounts at each step. In P_{700}-F_A/F_B complexes below 150 K, 75% of ET is blocked at or before A_1, which is similar to 69% in trehalose. And in both cases, only < 10% of electrons reach the terminal [4Fe-4S] clusters. The second is that F_X undergoes heterogeneous recombination, giving multiple lifetimes in the range of 500 μs to 10's of ms.

Similarities can also be seen in the amplitudes of the charge recombination components on lowering the temperature below 200 K for PS I in a water-glycerol solution (this study) and lowering the relative humidity below 60% for PS I in a trehalose glass [21] (Fig. 9). At relatively a high temperature/humidity, recombination occurs predominantly from the terminal F_A/F_B clusters, but on transition to the glassy state, its contribution decreases at the expense of an increase in the recombination from both F_X^- and A_1^-. Notably, while the majority of the recombination derives from A_1^- at $T < 150$ K, only a moderate

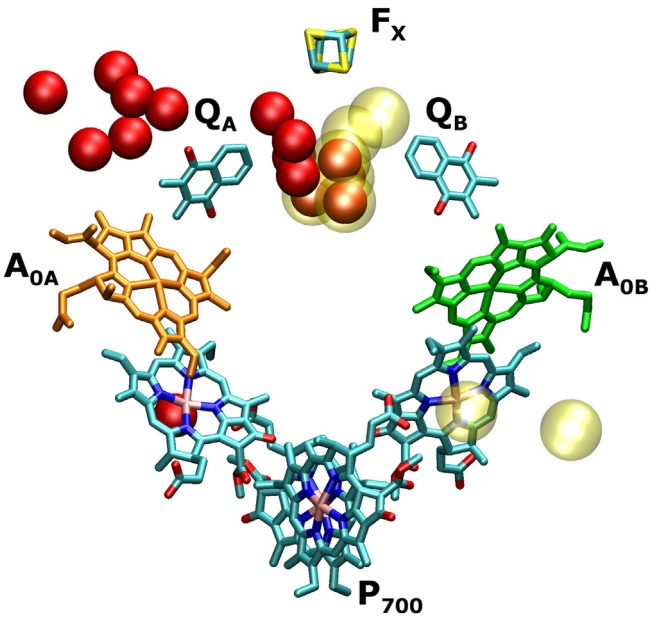

Fig. 10. Factors affecting the altered recombination in PS I embedded in a trehalose glassy matrix. Asymmetrically placed water molecules are shown as spheres. Water molecules within 15 Å of A_{1A} are shown in solid red, and those within 15 Å of A_{1B} are shown in transparent yellow spheres.

increase in the amplitude of this component occurs in the case of dry trehalose glass. We surmise that after gradual dehydration, the increase in the amount of recombination from F_X^- is observed at a relative humidity of 35–40%, while the increase of recombination from A_1^- only occurs at a relative humidity of at 11%. This difference may originate from the different arrangement of cofactors: while the [4Fe-4S] clusters are located on the periphery of PS I, close to the protein-water boundary, the A_1 binding sites are in the hydrophobic core of the protein. It is possible that at extreme levels of dehydration of the trehalose glassy matrix (11% humidity) some of the internal waters near A_{1A} and A_{1B} may be removed (Fig. 10). Their removal could alter the midpoint potential of the ET cofactors as well as the reorganization energy, thereby creating conditions that may render forward ET to the F_X cluster thermodynamically and/or kinetically unfavorable.

This retardation of ET in the trehalose and glycerol mixtures could be caused by similar physical processes that take place within and around the protein globule, namely, a glass transition of the surrounding medium. As described above, the temperature at which a sudden change of recombination kinetics in glycerol solution occurs (~170 K) corresponds to the glass transition temperature of 75% water-glycerol solution [35]. Room temperature (298 K) seems to be below the glass transition temperature for a 10% water-trehalose mixture but above the glass transition temperature for 30% water-trehalose mixture [63], so the process of dehydration also puts the solution through the glass transition process. It should be noted though that in the case of a low-temperature water-glycerol solution, the slowdown in ET is strongly affected by the activation energy of charge recombination (and corresponding differences in redox potentials), while this factor cannot be used for the interpretation of kinetic measurements in the dry trehalose matrix.

5. Conclusions

- Charge recombination reactions from the iron-sulfur clusters F_A/F_B and F_X, and from the PhQs A_{1A} and A_{1B} were distinguishable in P_{700}-F_A/F_B complexes and P_{700}-F_X cores of PS I from *Synechocystis* sp. PCC 6803 by their recombination kinetics with P_{700}^+. Forward ET to F_A/F_B was arrested below ~170 K, the glass transition temperature of the water-glycerol mixture. At temperatures below glass transition, ET was blocked at A_{1A}/A_{1B} and F_X (~60% and ~40% in P_{700}-F_A/F_B complexes and ~80% and ~20% in P_{700}-F_X cores, respectively).
- The kinetics of backward ET from all the acceptors to P_{700}^+ were found to be activation-less below the glass-transition temperature of ~170 K. Charge recombination from the iron-sulfur clusters at temperatures below 200 K were significantly heterogeneous in both P_{700}-F_A/F_B complexes and P_{700}-F_X cores. The F_X cluster was observed to be conformationally mobile in molecular dynamics simulations of PS I. The heterogeneity can be rationalized by preferential electron localization at different corners of the [4Fe-4S] cluster due to restricted conformational mobility of the surrounding polar medium. These effects, observed below the glass transition temperature, may account for the partial arrest of forward ET and the heterogeneity of charge recombination related to F_X.
- Two channels of charge recombination from the terminal iron-sulfur clusters are found in P_{700}-F_A/F_B complexes. Charge recombination by way of reverse ET to A_{1A} has an E_a of ~290 mV and is dominant at temperatures above ~280 K, whereas direct recombination from F_X^- with a low E_a of 22 mV is prevalent in the 200 to 270 K temperature range.
- The altered charge recombination at low temperatures is analogous to impeded ET in PS I complexes suspended in dry trehalose matrices at room temperature. The nature of the retardation of ET in these cases may differ, as temperature-dependent ET slowdown is mostly determined by the E_a of charge recombination (and corresponding differences in redox potential) while the trehalose matrix mainly restricts conformational mobility of the protein and may affect water molecules near the redox centers.

Transparency document

The Transparency document associated with this article can be found, in online version.

Acknowledgments

This work was supported by grant from Russian Foundation for Basic Research (grant number 17-00-00201, complex project 17-00-00218) to A.Yu.S. and by a grant from the U.S. National Science Foundation (MCB-16130222) to J.H.G. Molecular dynamics simulation of PS I was supported by grant from Russian Science Foundation (17-14-01323) to A.Yu.S.

Appendix A. Supplementary data

Supplementary data to this article can be found online at https://doi.org/10.1016/j.bbabio.2019.06.008.

References

[1] K. Brettel, Electron transfer and arrangement of the redox cofactors in photosystem I, Biochim. Biophys. Acta 1318 (1997) 322–373.
[2] K. Brettel, W. Leibl, Electron transfer in photosystem I, Biochim. Biophys. Acta 1507 (2001) 100–114.
[3] J. Golbeck, Photosystem I: The Light-Driven Plastocyanin:Ferredoxin Oxidoreductase, Springer, Dordrecht, The Netherlands, 2006.
[4] P. Fromme, P. Jordan, N. Krauß, Structure of photosystem I, Biochim. Biophys. Acta 1507 (2001) 5–31.
[5] I. Grotjohann, P. Fromme, Structure of cyanobacterial photosystem I, Photosynth. Res. 85 (2005) 51–72.
[6] P. Fromme, I. Grotjohann, Structure of photosystems I and II, Results Probl. Cell Differ. 45 (2008) 33–72.
[7] P. Bordier Høj, I. Svendsen, H. Vibe Scheller, B. Lindberg Møller, Identification of a chloroplast-encoded 9-kDa polypeptide as a 2[4Fe-4S] protein carrying centers A and B of photosystem I, J. Biol. Chem. 262 (1987) 12676–12684.
[8] N. Hayashida, T. Matsubayashi, K. Shinozaki, M. Sugiura, K. Inoue, T. Hiyama, The gene for the 9 kd polypeptide, a possible apoprotein for the iron-sulfur centers A and B of the photosystem I complex, in tobacco chloroplast DNA, Curr. Genet. 12 (1987) 247–250.

[9] R.M. Wynn, R. Malkin, Characterization of an isolated chloroplast membrane iron-sulfur protein and its identification as the photosystem I iron-sulfurA/iron-sulfurB binding protein, FEBS Lett. 229 (1988) 293–297.
[10] P. Jordan, P. Fromme, H.T. Witt, O. Klukas, W. Saenger, N. Krauß, Three dimensional structure of photosystem I at 2.5 Å resolution, Nature 411 (2001) 909–917.
[11] B. Kok, On the reversible absorption change at 705 nm in photosynthetic organisms, Biochim. Biophys. Acta 22 (1956) 399–401.
[12] B. Kok, W. Gott, Activation spectra of 700 mmu absorption change in photosynthesis, Plant Physiol. 35 (1960) 802–808.
[13] I.V. Shelaev, F.E. Gostev, M.D. Mamedov, O.M. Sarkisov, V.A. Nadtochenko, V.A. Shuvalov, A.Y. Semenov, Femtosecond primary charge separation in *Synechocystis sp*. PCC 6803 photosystem I, Biochim. Biophys. Acta 1797 (2010) 1410–1420.
[14] V.A. Shuvalov, A.V. Klevanik, A.V. Sharkov, P.G. Kryukov, K.E. Bacon, Picosecond spectroscopy of photosystem I reaction centers, FEBS Lett. 107 (1979) 313–316.
[15] J. Fajer, M.S. Davis, A. Forman, V.V. Klimov, E. Dolan, B. Ke, Primary electron acceptors in plant photosynthesis, J. Am. Chem. Soc. 102 (1980) 7143–7145.
[16] K. Brettel, Electron transfer from A_1^- to an iron-sulfur center with $t_{1/2}$ = 200 ns at room temperature in photosystem I. characterization by flash absorption spectroscopy, FEBS Lett. 239 (1988) 93–98.
[17] M. Guergova-Kuras, B. Boudreaux, A. Joliot, P. Joliot, K. Redding, Evidence for two active branches for electron transfer in photosystem I, Proc. Natl. Acad. Sci. U. S. A. 98 (2001) 4437–4442.
[18] N. Srinivasan, J.H. Golbeck, Protein-cofactor interactions in bioenergetic complexes: the role of the A_{1A} and A_{1B} phylloquinones in photosystem I, Biochim. Biophys. Acta 1787 (2009) 1057–1088.
[19] K. Sauer, P. Mathis, S. Acker, J.A. Van Best, Electron acceptors associated with P-700 in Triton solubilized photosystem I particles from spinach chloroplasts, Biochim. Biophys. Acta 503 (1978) 120–134.
[20] I.R. Vassiliev, Y.S. Jung, M.D. Mamedov, A. Semenov, J.H. Golbeck, Near-IR absorbance changes and electrogenic reactions in the microsecond-to-second time domain in photosystem I, Biophys. J. 72 (1997) 301–315.
[21] M. Malferrari, A. Savitsky, M.D. Mamedov, G.E. Milanovsky, W. Lubitz, K. Mobius, A.Y. Semenov, G. Venturoli, Trehalose matrix effects on charge-recombination kinetics in photosystem I of oxygenic photosynthesis at different dehydration levels, Biochim. Biophys. Acta 1857 (2016) 1440–1454.
[22] K.G. Parrett, T. Mehari, P.G. Warren, J.H. Golbeck, Purification and properties of the intact P-700 and Fx-containing photosystem I core protein, Biochim. Biophys. Acta 973 (1989) 324–332.
[23] K. Brettel, J.H. Golbeck, Spectral and kinetic characterization of electron acceptor A(1) in a photosystem I core devoid of iron-sulfur centers F_X, F_B and F_A, Photosynth. Res. 45 (1995) 183–193.
[24] D.A. Cherepanov, G.E. Milanovsky, O.A. Gopta, R. Balasubramanian, D.A. Bryant, A.Y. Semenov, J.H. Golbeck, Electron-phonon coupling in cyanobacterial photosystem I, J. Phys. Chem. B 122 (2018) 7943–7955.
[25] P. Sétif, P. Mathis, T. Vänngård, Photosystem I photochemistry at low temperature. Heterogeneity in pathways for electron transfer to the secondary acceptors and for recombination processes, Biochim. Biophys. Acta 767 (1984) 404–414.
[26] I. Ikegami, P. Setif, P. Mathis, Absorption studies of photosystem I photochemistry in the absence of vitamin K_1, Biochim. Biophys. Acta 894 (1987) 414–422.
[27] E. Schlodder, K. Falkenberg, M. Gergeleit, K. Brettel, Temperature dependence of forward and reverse electron transfer from A_1^-, the reduced secondary electron acceptor in photosystem I, Biochemistry 37 (1998) 9466–9476.
[28] R. Agalarov, K. Brettel, Temperature dependence of biphasic forward electron transfer from the phylloquinone(s) A1 in photosystem I: only the slower phase is activated, Biochim. Biophys. Acta 1604 (2003) 7–12.
[29] H. Makita, G. Hastings, Modeling electron transfer in photosystem I, Biochim. Biophys. Acta 1857 (2016) 723–733.
[30] K. Brettel, Electron transfer and arrangement of the redox cofactors in photosystem I, Biochim. Biophys. Acta Bioenerg. 1318 (1997) 322–373.
[31] V. Shinkarev, Functional modeling of electron transfer in photosynthetic reaction centers, in: J. Golbeck (Ed.), Photosystem I, Springer, Netherlands, 2006, pp. 611–637.
[32] R. Jordan, U. Nessau, E. Schlodder, Charge recombination between the reduced iron-sulphur clusters and P700, in: G. Garab (Ed.), Photosynthesis: Mechanisms and Effects, 1998, p. 663 (Budapest).
[33] G. Shen, M.L. Antonkine, A. van der Est, I.R. Vassiliev, K. Brettel, R. Bittl, S.G. Zech, J. Zhao, D. Stehlik, D.A. Bryant, J.H. Golbeck, Assembly of photosystem I. II. Rubredoxin is required for the *in vivo* assembly of F_X in *Synechococcus* sp. PCC 7002 as shown by optical and EPR spectroscopy, J. Biol. Chem. 277 (2002) 20355–20366.
[34] J.H. Golbeck, Resolution and reconstitution of photosystem I, in: P.S. Song, W.M. Horspool (Eds.), CRC Handbook of Organic Photochemistry and Photobiology, CRC Press, Bocca Raton, FL, 1995, pp. 1407–1419.
[35] D.H. Rasmussen, A.P. MacKenzie, The glass transition in amorphous water. Application of the measurements to problems arising in cryobiology, J. Phys. Chem. 75 (1971) 967–973.
[36] S.W. Provencher, Contin - a general-purpose constrained regularization program for inverting noisy linear algebraic and integral-equations, Comput. Phys. Commun. 27 (1982) 229–242.
[37] W.D. Cornell, P. Cieplak, C.I. Bayly, I.R. Gould, K.M. Merz, D.M. Ferguson, D.C. Spellmeyer, T. Fox, J.W. Caldwell, P.A. Kollman, A 2nd generation force-field for the simulation of proteins, nucleic acids, and organic molecules, J. Am. Chem. Soc. 117 (1995) 5179–5197.
[38] L. Zhang, D.-A. Silva, Y. Yan, X. Huang, Force field development for cofactors in the photosystem II, J. Comput. Chem. 33 (2012) 1969–1980.
[39] B. Hess, C. Kutzner, D. Van Der Spoel, E. Lindahl, GRGMACS 4: algorithms for highly efficient, load-balanced, and scalable molecular simulation, J. Chem. Theory Comput. 4 (2008) 435–447.
[40] W. Humphrey, A. Dalke, K. Schulten, VMD: visual molecular dynamics, J. Mol. Graph. 14 (1996) 33–38 (27-38).
[41] G.E. Milanovsky, V.V. Ptushenko, J.H. Golbeck, A.Y. Semenov, D.A. Cherepanov, Molecular dynamics study of the primary charge separation reactions in photosystem I: effect of the replacement of the axial ligands to the electron acceptor A0, Biochim. Biophys. Acta 1837 (2014) 1472–1483.
[42] S. Santabarbara, P. Heathcote, M.C. Evans, Modelling of the electron transfer reactions in photosystem I by electron tunnelling theory: the phylloquinones bound to the PsaA and the PsaB reaction centre subunits of PS I are almost isoenergetic to the iron-sulfur cluster F(X), Biochim. Biophys. Acta 1708 (2005) 283–310.
[43] H. Ishikita, E.W. Knapp, Redox potential of quinones in both electron transfer branches of photosystem I, J. Biol. Chem. 278 (2003) 52002–52011.
[44] V.V. Ptushenko, D.A. Cherepanov, L.I. Krishtalik, A.Y. Semenov, Semi-continuum electrostatic calculations of redox potentials in photosystem I, Photosynth. Res. 97 (2008) 55–74.
[45] V. Kurashov, M. Gorka, G.E. Milanovsky, T.W. Johnson, D.A. Cherepanov, A.Y. Semenov, J.H. Golbeck, Critical evaluation of electron transfer kinetics in P700-F_A/F_B, P700-F_X, and P700-A_1 photosystem I core complexes in liquid and in trehalose glass, Biochim. Biophys. Acta Bioenerg. 1859 (2018) 1288–1301.
[46] H. Makita, G. Hastings, Directionality of electron transfer in cyanobacterial photosystem I at 298 and 77 K, FEBS Lett. 589 (2015) 1412–1417.
[47] R. Malkin, A.J. Bearden, Primary reactions of photosynthesis: photoreduction of a bound chloroplast ferredoxin at low temperature as detected by EPR spectroscopy, Proc. Natl. Acad. Sci. U. S. A. 68 (1971) 16–19.
[48] A.R. McIntosh, M. Chu, J.R. Bolton, Flash photolysis electron spin resonance studies of the electron acceptor species at low temperatures in photosystem I of spinach subchloroplast particles, Biochim. Biophys. Acta 376 (1975) 308–314.
[49] E. Schlodder, K. Falkenberg, M. Gergeleit, K. Brettel, Temperature dependence of forward and reverse electron transfer from A_1^-, the reduced secondary electron acceptor in photosystem I, Biochemistry 37 (1998) 9466–9476.
[50] P. Setif, P. Mathis, T. Vaenngaard, Photosystem I photochemistry at low temperature. Heterogeneity in pathways for electron transfer to the secondary acceptors and for recombination processes, Biochim. Biophys. Acta 767 (1984) 404–414.
[51] S. Santabarbara, I. Kuprov, P.J. Hore, A. Casal, P. Heathcote, M.C. Evans, Analysis of the spin-polarized electron spin echo of the [P700+ A1-] radical pair of photosystem I indicates that both reaction center subunits are competent in electron transfer in cyanobacteria, green algae, and higher plants, Biochemistry 45 (2006) 7389–7403.
[52] S. Santabarbara, I. Kuprov, O. Poluektov, A. Casal, C.A. Russell, S. Purton, M.C. Evans, Directionality of electron-transfer reactions in photosystem I of prokaryotes: universality of the bidirectional electron-transfer model, J. Phys. Chem. B 114 (2010) 15158–15171.
[53] H. Makita, N. Zhao, G. Hastings, Time-resolved visible and infrared difference spectroscopy for the study of photosystem I with different quinones incorporated into the A_1 binding site, Biochim. Biophys. Acta 1847 (2015) 343–354.
[54] D. Kleinfeld, M.Y. Okamura, G. Feher, Electron-transfer kinetics in photosynthetic reaction centers cooled to cryogenic temperatures in the charge-separated state: evidence for light-induced structural changes, Biochemistry 23 (1984) 5780–5786.
[55] R. Bittl, S.G. Zech, P. Fromme, H.T. Witt, W. Lubitz, Pulsed EPR structure analysis of photosystem I single crystals: localization of the phylloquinone acceptor, Biochemistry 36 (1997) 12001–12004.
[56] A. Savitsky, O. Gopta, M. Mamedov, J.H. Golbeck, A. Tikhonov, K. Mobius, A. Semenov, Alteration of the axial met ligand to electron acceptor A_0 in photosystem I: effect on the generation of $P_{700}^{\bullet+}$ $A_1^{\bullet-}$ radical pairs as studied by W-band transient EPR, Appl. Magn. Reson. 37 (2010) 85–102.
[57] E.L. Bominaar, C. Achim, S.A. Borshch, J.J. Girerd, E. Munck, Analysis of exchange interaction and electron delocalization as intramolecular determinants of intermolecular electron-transfer kinetics, Inorg. Chem. 36 (1997) 3689–3701.
[58] H.J. Hou, D. Mauzerall, The A^-F_X to $F_{(A/B)}$ step in *Synechocystis* 6803 photosystem I is entropy driven, J. Am. Chem. Soc. 128 (2006) 1580–1586.
[59] J.H. Golbeck, K.G. Parrett, T. Mehari, K.L. Jones, J.J. Brand, Isolation of the intact photosystem I reaction center core containing P700 and iron-sulfur center FX, FEBS Lett. 228 (1988) 268–272.
[60] N.K. Jain, I. Roy, Effect of trehalose on protein structure, Protein Sci. 18 (2009) 24–36.
[61] J.G. Sampedro, S. Uribe, Trehalose-enzyme interactions result in structure stabilization and activity inhibition. The role of viscosity, Mol. Cell. Biochem. 256-257 (2004) 319–327.
[62] I. Shelaev, M. Gorka, A. Savitsky, V. Kurashov, M. Mamedov, F. Gostev, K. Mobius, V. Nadtochenko, J. Golbeck, A. Semenov, Effect of dehydrated trehalose matrix on the kinetics of forward electron transfer reactions in photosystem I, Z. Phys. Chem. 231 (2017) 325–345.
[63] J.G. Constantin, M. Schneider, H.R. Corti, Glass transition temperature of saccharide aqueous solutions estimated with the free volume/percolation model, J. Phys. Chem. B 120 (2016) 5047–5055.